Compaction of Cohesive Powders

Dietrich E. Wolf & Tamás Unger & Dirk Kadau & Lothar Brendel
Department of Physics, University Duisburg-Essen, Germany

The finer a powder, the more its behaviour is dominated by cohesion. This is the reason why fine powders in the submicrometer range are highly porous. The stress that is needed to reduce the porosity by a desired amount is shown to be different in quasi-static and in shock compaction. The product of (consolidation stress)·(compactible pore volume)$^{1/\alpha}$ turns out to be constant for a powder of rigid, round particles with an exponent $1/\alpha \approx 2$. How this constitutive law is modified in the case of shock compaction due to inertia effects, is derived analytically. Results of Contact Dynamics simulations and experiments are reviewed.

1 INTRODUCTION

The flow of fine powders in the micrometer and submicrometer range is strongly influenced by cohesion. For instance, a fine powder does not collapse into a random dense packing under its own weight (Fig. 1): Its porosity depends on the preparation history and can be as large as 90%.

Cohesion is particularly important in nano-powder and aerosol technology. As an example, Fig. 2 shows a snapshot from a simulation (Hänel & Lantermann 2005) of nanoparticles carried by a gas through a filter, where some of them are deposited, forming flakes which have a structure similar to ballistic deposits (Vold 1959; Jullien & Meakin 1989).

In order to obtain a nano-crystalline solid one has to avoid sintering at high temperature, because it would lead to coarsening of the crystallites. Instead one applies high pressure to compactify the porous nano-powder (Srdić et al. 2000). Another important application is the compaction of cohesive medical powders into tablets (Masteau et al. 1997). Here we review recent progress made in understanding the compaction of cohesive powders (Kadau et al. 2003; Brendel et al. 2003; Bartels et al. 2005) and present new results concerning the relation between quasi-static and shock compaction.

The van-der-Waals attraction leads to solid necks between particles which form instantaneously due to elastic deformation, when two particles come into contact (Johnson et al. 1971). These necks can have an initial diameter of half the particle radius for nanoparticles and subsequently grow by surface and grain boundary diffusion (see e.g. Westerhoff (2005)). Relative motion at such a contact is assumed in the following to require that tensile or shear forces exceed a threshold at which the solid bridge connecting the two particles breaks. Moreover instantaneous formation of a solid neck is assumed whenever a contact forms. Slow aging or sintering which reinforce long lived solid bridges beween particles are not taken into account here.

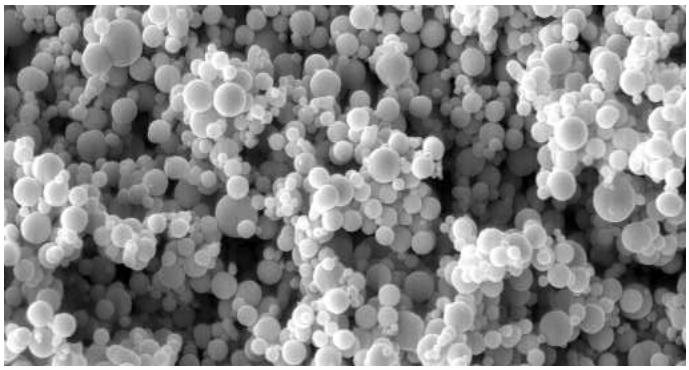

Figure 1. Electron microscope image of carbonyl-iron-powder with typical particle radius of 1μm.

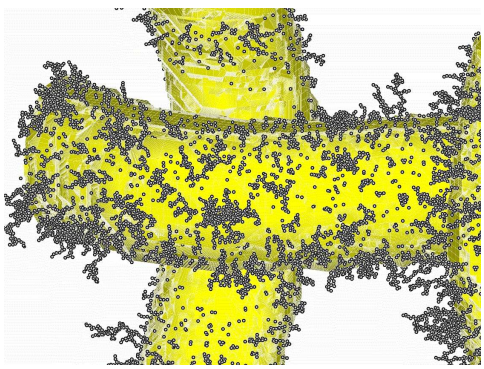

Figure 2. Nano-particles filtered from the gas phase. Simulation by U. Lantermann (2002).

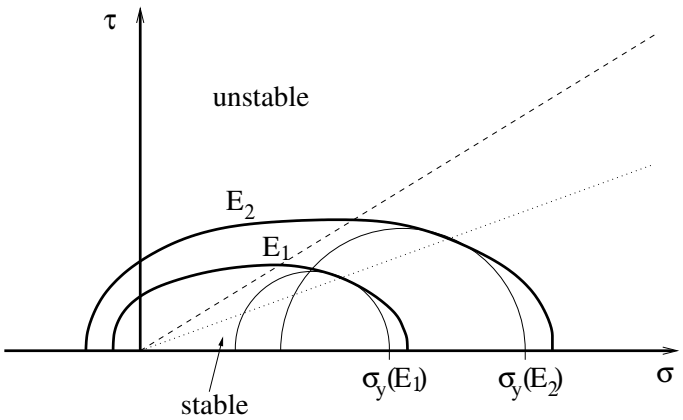

Figure 3. Simplified view of the stability regions of a cohesive powder for two different porosities, $E_1 > E_2$. Where the boundary of the stability region intersects the Roscoe line (dashed), one gets steady state flow. The point, where uniaxial compaction sets in, is the intersection of the stability boundary with the dotted curve. The Mohr-circle tangential to the stability boundary at such a point intersects the σ-axis at the principal stresses characteristic for quasi-static uniaxial compaction of a powder of the corresponding porosity. The larger one, σ_y, is the stress at the piston in the experiments described in the text.

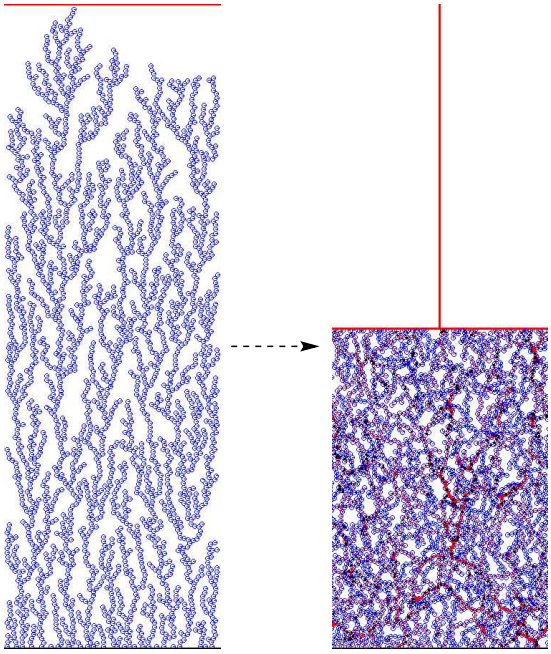

Figure 4. Initial and final configuration of simulated uniaxial compaction with given stress σ_y at the piston.

2 THE GENERAL FRAMEWORK

One commonly assumes that a cohesive powder with a given porosity sustains stationary combinations of shear and normal stresses within a convex region, the "stability region", in (σ, τ)-space, Fig. 3 (Roscoe 1970; Schwedes 1975). σ is the normal and τ the tangential force per unit area transmitted through a plane with normal vector $\vec{n}$ inside the material. (Tensile forces are defined as being negative here.) Usually one assumes that the material is isotropic. Then only vectors $\vec{n}$ that are linear combinations of the eigenvectors for the largest and smallest eigenvalue of the stress tensor are taken into account, because the corresponding Mohr circle is largest and therefore reaches the boundary of the stability region first. Quasi-static compaction takes place at the boundary of the stability region. We shall also discuss shock compaction in this paper, where a load in the unstable region is applied.

This picture is certainly oversimplified: Porosity is not the only property of the cohesive powder that determines to what stresses it yields. Moreover, it was shown in recent simulations of non-cohesive, polygonal, elastic particles that periodically varying stresses inside the stability region cause local, irreversible particle displacements (*ratcheting*), which can accumulate on long time scales to macroscopic deformations (Alonso-Marroquín & Herrmann 2004).

We did Contact Dynamics simulations of cohesive, rigid particles with Coulomb friction, rolling friction (and in three dimensions torsion friction, as well (Bartels et al. 2005)). An introduction to the simulation method is given in (Brendel et al. 2004). Figure 4 shows the initial and the final configuration of a two-dimensional simulation of uniaxial compaction (Kadau 2003): A piston pushes downwards (y-direction) with a given force, while the lateral system size (x-direction) is kept fixed. As friction at the bottom and at the piston is set equal to zero in the simulation, and periodic boundary conditions are used in the x-direction, the principal axes of the stress tensor must be the x- and y-direction. Therefore we denote the eigenvalues by σ_x and σ_y, the latter being the stress exerted by the piston.

From experiments (Nowak 1994) it is known that the eigenvalues of the stress are proportional to each other. We confirmed this in our simulations by moving the piston with a fixed velocity and measuring σ_y as well as σ_x as the powder becomes denser and denser. The result is shown in Fig. 5.

Parallel to our simulations, experiments were done by Morgeneyer and Schwedes (Morgeneyer 2004), who compactified carbonyl-iron powder (Fig. 1) uniaxially by means of a true biaxial shear tester (Schwedes 2003). Here too, wall friction was practically eliminated by covering the walls with lubricated elastic membranes. Carbonyl-iron powder consists of spherical iron particles which are very rigid. Therefore it serves as a model substance for comparison with Contact Dynamics simulations.

The density of a powder can be quantified by its solid fraction ν, which is the ratio between the solid volume and the total volume, or by the porosity,

$$E = 1 - \nu \,. \tag{1}$$

Extrapolating to infinite stress at the piston, the minimal porosity $E_{\min}$ of a powder of perfectly rigid particles is not zero. As we shall see below, from a theoretical point of view it turns out to be convenient to use

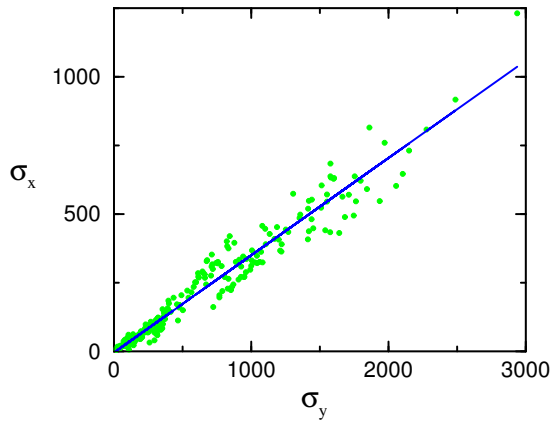

Figure 5. In strain controlled uniaxial compaction the principal stresses increase proportional to each other.

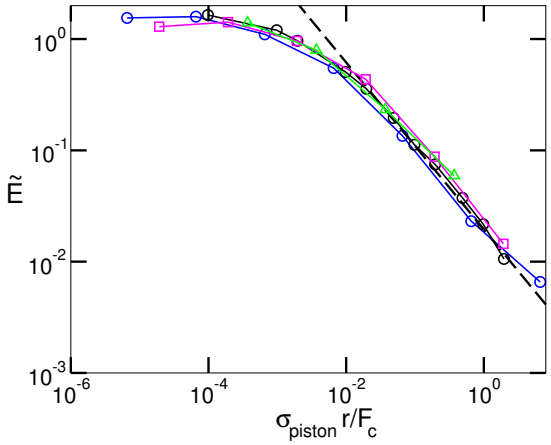

Figure 6. Log-log-plot of the final volume excess, Eq. (2), as a function of the dimensionless stress at the piston for a two-dimensional simulation of shock compaction. For large stress, $\tilde{E}$ vanishes with a power law. Dashed line has slope $-3/4$.

the relative compactible pore volume, instead, which we call "volume excess":

$$\tilde{E} \equiv \frac{V - V_{\min}}{V_{\min}} = \frac{\nu_{\max}}{\nu} - 1 = \frac{E - E_{\min}}{1 - E} , \qquad (2)$$

where the last transformation results from inserting Eq. (1). $V_{\min}$ is the minimal volume a powder sample of rigid particles can have, when compacted uniaxially with infinite pressure. (The variation of $V_{\min}$ for different random dense packings is small enough that it may be neglected here.) In the simulations we determined $V_{\min}$ by switching off cohesion and rolling friction so that any nonzero stress exerted by the piston leads to maximal compaction.

In the experiments with the biaxial shear tester the sample was always near the stability limit (*quasi-static compaction*). The stress at the piston could therefore be identified with the consolidation stress $\sigma_y(\tilde{E})$ for the current volume excess or porosity (see Fig. 3).

By contrast, in the simulation, the same initial configuration was subjected to different stresses σ_{piston}, which could exceed the consolidation stress by a factor of 100 or even 1000: The simulated compaction is then far from quasi-static (*shock compaction*). This gives rise to inertia effects, which will be discussed in Sections 5 to 7. As a consequence one arrives at the desired compaction with a *smaller* stress than in the quasi-static case.

3 THE COMPACTION LAW

In this section the question is anwered, down to what value the volume excess decreases, when a certain stress is applied at the piston. At first one has to realize that $\tilde{E}$, like porosity or solid fraction, is dimensionless, while the stress is not. Therefore an intrinsic stress scale is needed which enables us to dedimensionalize σ. For perfectly rigid particles the only parameter combination with this property is the cohesion force F_c between two particles divided by the particle radius squared (in three dimensions). We conclude that the volume excess must be a function of the dimensionless stress

$$\tilde{\sigma} = \frac{\sigma r^{d-1}}{F_c} , \qquad (3)$$

where d denotes the space dimension, which in the simulations presented here was 2. Equation (3) explains why the compaction of nano powders requires much larger stresses (several Mega-Pascal) than for powders in the micrometer range (kilo-Pascal). Of course there are other dimensionless quantities, on which the volume excess can depend in addition, such as aspect ratio of the system, friction coefficients, particle shape parameters (Kadau et al. 2003), and the fabric (Radjai & Roux 2004).

Figure 6 shows simulation data for four systems. The initial configurations were ballistic deposits like in Fig. 4 with the same solid fraction. The particles were round and had all the same size. The coefficients of Coulomb and rolling friction were the same in all four systems. The systems differed by their aspect ratio (L_y/L_x between 1 and 4), total particle number (between 242 and 2746) and piston mass (between 0.1 and 1.7 times the total mass of all particles). The dependence on these dimensionless parameters is obviously much weaker than the dependence on the dimensionless stress.

For small stress the volume excess remains essentially unchanged. Around a characteristic stress value, which we identify with the consolidation stress for the initial configuration, the volume excess crosses over into a power law. For larger stresses we find (Kadau 2003)

$$\tilde{E} \sim \tilde{\sigma}_{\text{piston}}^{-\beta} \qquad \text{(shock compaction)} \qquad (4)$$

with an exponent $\beta \approx 3/4$.

Such a crossover into a power law was subsequently also found in quasi-static experiments (Brendel et al. 2003; Morgeneyer 2004). For the analysis of

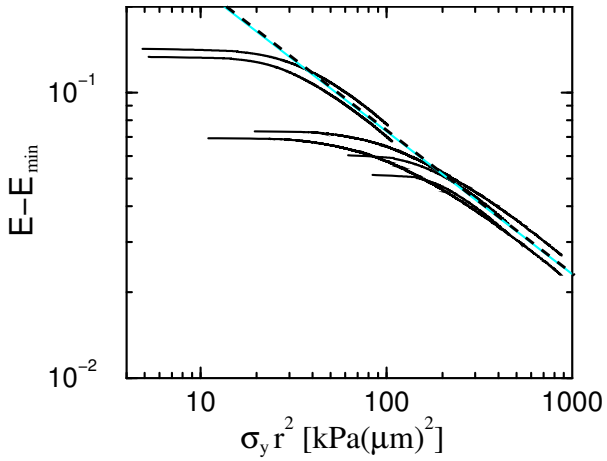

Figure 7. Experimental results for three carbonyl-iron powders with particle diameters of about 2, 4, and 6 μm, respectively, and different initial porosities (Morgeneyer 2004). For large stress the porosity E approaches its minimal value with a power law. Dashed line has slope $-1/2$.

the data obtained with the biaxial shear tester (Fig. 7) it is very important to have additional microscopic information about the radius dependence of the cohesion force between the particles. This information was provided by atomic force measurements on individual particles from the three carbonyl-iron-powder samples (Heim 2005). Each sample had a rather narrow distribution of the particle diameters around 2, 4 and 6 μm. It turns out, that the cohesion force for particles from the three samples is dominated by the particle roughness, so that no significant radius dependence can be found. According to the definition of the dimensionless stress, Eq. (3), one can therefore expect that the porosity depends on $\sigma_y r^2$. Extrapolating slightly different minimal porosities for the limit of infinite stress for the three samples, the data can be presented in the form of Fig. 7. As the difference $E - E_{\text{min}}$ is in first order proportional to the volume excess $\tilde{E}$, one obtains for large stress the power law

$$\tilde{E} \sim \tilde{\sigma}_y^{-\alpha} \qquad (\text{quasi} - \text{static comp.}) \qquad (5)$$

with an exponent $\alpha \approx 1/2$.

This raises the question, whether the exponents α for quasi-static compaction and β for shock compaction are the same. The answer, which will be derived below in Sec. 8, is that the two exponents are *not* equal: $\beta = \alpha(1+\alpha)$. The value of $\beta \approx 3/4$ obtained in the simulations of two dimensional shock compaction therefore implies $\alpha \approx 1/2$ for two dimensional quasi-static compaction. This happens to agree with the exponent found in the three-dimensional experiments with carbonyl-iron-powder. Preliminary results from three-dimensional simulations of shock compaction (Johnson & Wolf 2005) indeed support the relation between β and α.

4 COMPARISON OF COMPACTION LAWS

In (Kawakita & Lüdde 1970) experimental results for the porosity E led to a compaction law which can be written as

$$E = \frac{E_0}{(1-E_0)\sigma/\sigma^* + 1} \,. \qquad (6)$$

This equation means that E approaches the initial porosity E_0 for $\sigma \ll \sigma^*$ and drops to zero as a power law with exponent $\alpha = -1$ for $\sigma \gg \sigma^*$. The characteristic stress σ^* should be identified with the consolidation stress. This equation describes the smooth crossover between the two regimes. It does not agree with our findings in several respects: The exponent is different, the porosity depends on the initial one even for large stress, an arbitrarily small stress suffices to make a powder denser no matter how much precompacted it already is, and the asymptotic porosity is assumed to be $E_{\text{min}} = 0$.

The equation reported by (Masteau et al. 1997),

$$\left(\frac{E}{1-E}\right)^{1-a} - \left(\frac{E_0}{1-E_0}\right)^{1-a} = \sigma/\sigma^* \,, \qquad (7)$$

where $a = 2$, differs from our results in the same respects as Eq. (6). Note, however, that our results were obtained for rigid, round particles.

5 THE DYNAMICS OF SHOCK COMPACTION

In order to compare the simulation results with quasi-static experiments one needs to understand the dynamical implications of shock compaction. The piston accelerates for a short time until it reaches a velocity v

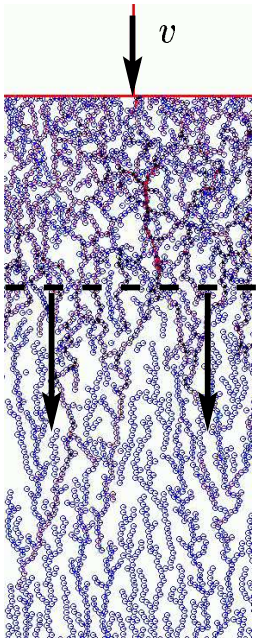

Figure 8. Snapshot of simulated shock compaction due to a sudden increase of σ_{piston}. The front between the regions of high and low porosity can be clearly seen.

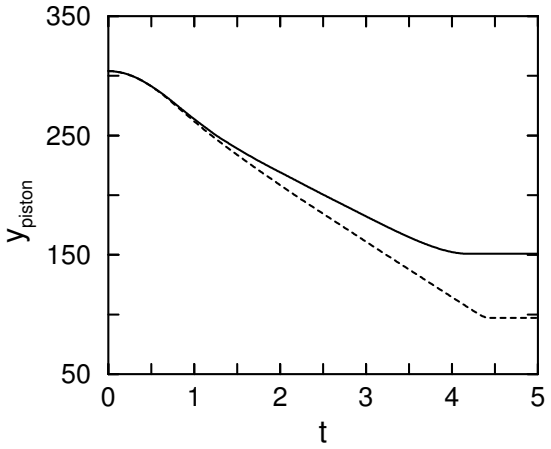

Figure 9. Piston position as a function of time t. Full line: Simulation with cohesion, Coulomb friction and rolling friction. The final piston position reached, when cohesion and rolling friction are switched off (dashed line), was used to calculate $V_{\min}$ for the definition of the volume excess. For increasing stress at the piston the solid line will come down to the dashed one.

which remains approximately constant (Fig. 9), while a compaction front runs through the system (Fig. 8). It separates a compacted region (solid fraction $\nu_1 > \nu_0$) in front of the piston, moving at velocity v, from the yet uncompacted part of the system (solid fraction ν_0), which is still at rest. The mass through which the front propagates, gets *compactified and accelerated*. Therefore we call it the "*acceleration front*". It is not mathematically sharp, but should interpolate smoothly between the two regions. The slower the piston moves, the wider the transition region is expected to be. In the quasi-static case it should span the whole system, so that one cannot speak of a "front" any more. Here we consider high compaction velocities, however, where the acceleration front is reasonably narrow.

When the acceleration front reaches the bottom wall opposite the piston, the whole powder moves at a velocity v together with the piston. In order to stop it instantaneously, an infinite force would be required. Such a force cannot be sustained by the powder so that a second, reflected compaction front moves towards the piston and stops it, provided the piston mass is zero. (The influence of a finite piston mass will be discussed briefly in the conclusion, Sec. 10.) This time the mass through which the front propagates, gets *compactified and stopped*. Therefore we call it the "*deceleration front*".

6 THE ACCELERATION FRONT

The following theory describes the regime, where the piston moves at constant velocity. Furthermore, the acceleration front is idealized as mathematically sharp.

During a short time interval δt the piston moves a distance $v\delta t$, and the acceleration front propagates a distance δy into the not yet compacted region, compacting it from solid fraction ν_0 to ν_1. Mass conservation relates the two lengths:

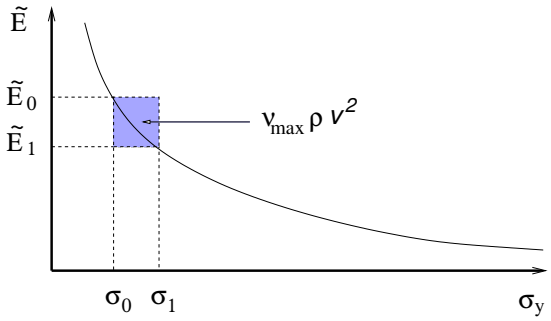

Figure 10. The constitutive law, Eq. (5), which relates the volume excess $\tilde{E}$ to the uniaxial consolidation stress σ_y, determines the velocity v of the piston, if the stress at the piston is suddenly raised from $\sigma_0 = \sigma_y(\tilde{E}_0)$ to σ_1.

$$v\delta t = \delta y \left(1 - \frac{\nu_0}{\nu_1}\right) . \tag{8}$$

In our simplified view only the slab of width δy with mass

$$\delta M = \rho \nu_0 A \delta y \tag{9}$$

(ρ being the mass density of the particles and A the piston area) changes its momentum during the time interval δt. This slab divides the system into two parts. The one next to the piston is already compacted to solid fraction ν_1 and therefore transmits the compaction stress σ_1. The region far from the piston, however, still has the smaller solid fraction ν_0, hence sustains only the stress σ_0. The momentum balance for the slab in between therefore reads

$$(\sigma_1 - \sigma_0) A \delta t = \delta M \; v \; . \tag{10}$$

Inserting Eqs. (8) and (9) results in a simple relation between the piston velocity v and the change of volume excess, which is the main result of this section:

$$\rho v^2 \;\; = \;\; (\tilde{E}_0 - \tilde{E}_1)(\sigma_1 - \sigma_0)/\nu_{\max} \tag{11}$$

Eq. (11) shows that the piston velocity is in leading order linear in the difference between the stress at the piston σ_1 and the quasi-static consolidation stress σ_0. Fig. 10 illustrates the result Eq. (11) schematically.

The work done by the piston in the time interval δt, $\sigma_1 A v \delta t$, is partly converted into kinetic energy, $\delta M v^2/2$. The rest is dissipated as heat during the irreversible compaction process:

$$\sigma_1 A v \delta t = \frac{1}{2}\delta M v^2 + \delta E_{\text{diss}} \; . \tag{12}$$

Inserting Eq. (10) an expression for the compaction work of a slab of mass δM is obtained, the second important result of this section:

$$\begin{aligned} \delta E_{\text{diss}} \;\; &= \;\; \frac{1}{2}\delta M v^2 + \sigma_0 v \delta t \\ &= \;\; \delta M \left(\frac{1}{2}\, v^2 + \frac{\sigma_0\, (\tilde{E}_0 - \tilde{E}_1)}{\rho \nu_{\max}} \right) . \end{aligned} \tag{13}$$

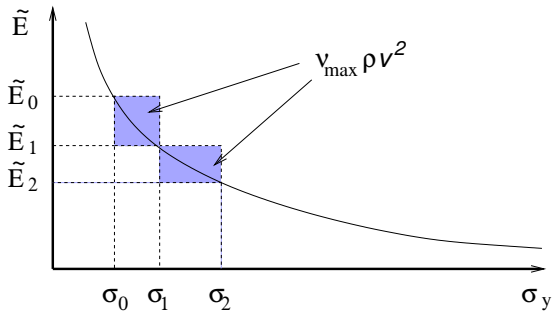

Figure 11. The deceleration front reduces the volume exess further to $\tilde{E}_2$, compare Fig. 10. σ_1 is the stress at the piston.

7 THE DECELERATION FRONT

If one considers the system in the comoving frame of the piston, the piston and the powder are at rest, when the acceleration front reaches the bottom wall. The bottom wall having infinite mass runs with an velocity $-v$ into the powder and compactifies it further to a solid fraction $\nu_2 > \nu_1$ while accelerating it to the same velocity (which in the laboratory frame means that the powder comes to rest). Now the stress near the bottom wall is $\sigma_2 > \sigma_1$ and drops to σ_1 on the other side of the deceleration front, near the piston. $\tilde{E}_2$ and σ_2 are determined by

$$\rho v^2 = \left(\tilde{E}_1 - \tilde{E}_2\right)(\sigma_2 - \sigma_1)/\nu_{\max} \qquad (14)$$

and the constitutive law (5) (Fig. 11). The compaction work

$$\delta E_{\rm diss} = \delta M \left(\frac{1}{2}\, v^2 + \frac{\sigma_1\,(\tilde{E}_1 - \tilde{E}_2)}{\rho \nu_{\max}}\right) . \qquad (15)$$

is partly provided by the kinetic energy of the powder (first term) and by the piston whose motion reduces the container volume accordingly (second term).

The combined action of the acceleration and the deceleration front leads to a final solid fraction ν_2 which is *larger* than expected from the stress at the piston, σ_1. A further compaction requires a stress larger than σ_2, the uniaxial consolidation stress of a powder of solid fraction ν_2.

The simulation results presented here therefore do *not* represent the constitutive law for the consolidation stress as function of the volume excess ($\sigma_2 = \sigma_y(\tilde{E}_2)$), as obtained in quasi-static experiments, but the relation between the stress σ_1 at the piston and the final volume excess $\tilde{E}_2$. Note that $\tilde{E}_2$ depends not only on σ_1 but also on the velocity v, therefore on the initial volume excess $\tilde{E}_0$. The final porosities obtained in the simulation belong to consolidation stresses that are systematically larger than the stress exerted by the piston. A crucial test of this idea will be a simulation, which successively compactifies the same system further and further by slowly incrementing the stress at the piston, rather than confronting always the uncompacted initial configuration with a stress, which run after run is increased far beyond the consolidation stress.

The theory allows to compare the energy dissipated in shock compaction of a cohesive powder with the one in quasi-static compaction, both from volume excess $\tilde{E}_0$ to $\tilde{E}_2$. The energy dissipated in shock compaction is

$$E_{\rm diss}^{\rm (shock)} = \sigma_1 V_{\min}(\tilde{E}_0 - \tilde{E}_2)\,, \qquad (16)$$

whereas in the quasi-static case it is

$$E_{\rm diss}^{\rm (qs)} = V_{\min} \int_{\tilde{E}_2}^{\tilde{E}_0} \sigma_y(\tilde{E}) d\tilde{E}\,, \qquad (17)$$

which is the area left of the curved line in Fig. 11 between $\tilde{E}_0$ and $\tilde{E}_2$. Due to its curvature the line $\sigma_y(\tilde{E})$ cuts the shaded rectangles into a larger upper and a smaller lower part. It follows immediately that the lower part of the right rectangle does not suffice to fill the upper part of the left rectangle: As expected, shock compaction costs more energy than quasi-static compaction.

8 RELATION BETWEEN QUASI-STATIC AND SHOCK COMPACTION

As pointed out in the previous section, the stress σ_1 which must be applied at the piston in order to compactify the powder by a desired amount depends both on the initial and the final volume excess, $\tilde{E}_0 > \tilde{E}_2$, due to inertia effects. It is systematically smaller than the stress $\sigma_2 = \sigma_y(\tilde{E}_2)$ at which $\tilde{E}_2$ would be reached quasi-statically.

In our simulations we determined the function $\sigma_1 = \sigma_{\rm piston}(\tilde{E}_0, \tilde{E}_2)$ by measuring $\tilde{E}_2$ for given σ_1 and $\tilde{E}_0$, and we found that

$$\frac{1}{\sigma_{\rm piston}(\tilde{E}_0, \tilde{E}_2)} \sim \frac{r^2}{F_c} \tilde{E}_2^{1/\beta}\, f(\tilde{E}_0) \qquad (18)$$

in the limit of large $\sigma_{\rm piston}$. In this section we shall derive the exponent β and the function $f(\tilde{E}_0)$ from the quasi-static compaction law

$$\frac{1}{\sigma_i} = \frac{1}{\sigma_y(\tilde{E}_i)} \sim \frac{r^2}{F_c} \tilde{E}_i^{1/\alpha}, \quad i = 0, 1, 2, \qquad (19)$$

using the theory developed in the previous two sections. The result will be that

$$\beta = \alpha(1+\alpha)\,, \quad f(\tilde{E}_0) = \tilde{E}_0^{1/(1+\alpha)}\,. \qquad (20)$$

The equal area condition for the two shaded rectangles in Fig. 11 implies that

$$\sigma_1(\tilde{E}_0 - \tilde{E}_2) = \sigma_0(\tilde{E}_0 - \tilde{E}_1) + \sigma_2(\tilde{E}_1 - \tilde{E}_2)\,. \qquad (21)$$

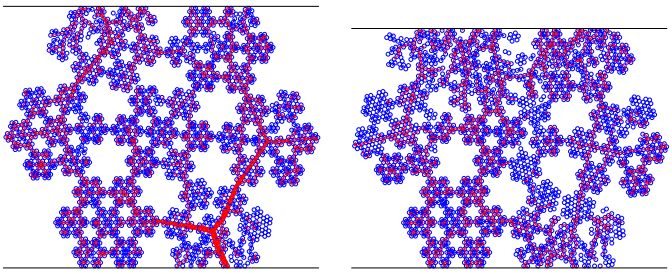

Figure 12. A fractal initial configuration subjected to a stress above the stability limit remains nearly unchanged for some time, before it starts to collapse. Width of lines connecting particle centers indicates strength of the contact force between them.

σ_0 and the terms in brackets remain finite for diverging σ_1, so that asymptotically the first term on the right hand side can be neglected:

$$\frac{1}{\sigma_1}\,(\tilde{E}_1 - \tilde{E}_2) \approx \frac{1}{\sigma_2}\,(\tilde{E}_0 - \tilde{E}_2)\,. \qquad (22)$$

Inserting Eq. (19) leads to

$$\tilde{E}_1^{1/\alpha}\,(\tilde{E}_1 - \tilde{E}_2) \approx \tilde{E}_2^{1/\alpha}\,(\tilde{E}_0 - \tilde{E}_2)\,. \qquad (23)$$

As the bracket on the right hand side remains finite while the one on the left hand side goes to zero, $\tilde{E}_1$ must be much larger than $\tilde{E}_2$. Hence one must identify in leading order

$$\tilde{E}_1^{1/\alpha\,+1} \approx \tilde{E}_2^{1/\alpha}\tilde{E}_0\,. \qquad (24)$$

Inserting this into $1/\sigma_1$, Eq. (19), gives

$$\frac{1}{\sigma_{\rm piston}(\tilde{E}_0,\tilde{E}_2)} = \frac{r^2}{F_c}\tilde{E}_2^{\frac{1}{\alpha}-\frac{1}{1+\alpha}}\,\tilde{E}_0^{\frac{1}{1+\alpha}} \qquad (25)$$

which by comparison with Eq. (18) completes the proof of Eq. (20).

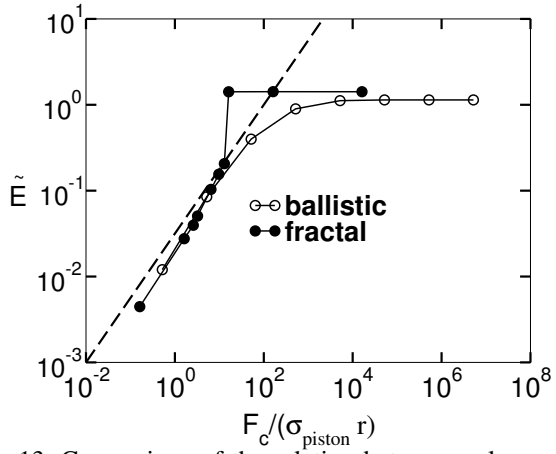

Figure 13. Comparison of the relation between volume excess and inverse dimensionless stress at the piston for a fractal initial configuration and a ballistic deposit. Dashed line has slope 3/4.

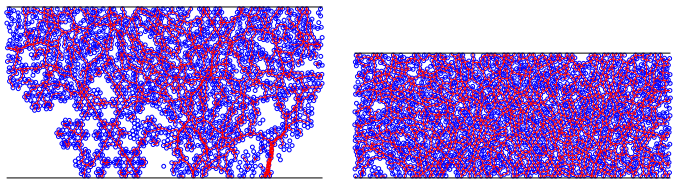

Figure 14. The collapse of the fractal structure under a given stress at the piston leads to a final, essentially homogeneous porosity. Further compaction of the final configuration follows the same laws as derived in Secs. 5 – 8.

9 COMPACTION OF A FRACTAL

The simulation results Fig. 6 and Fig. 9 were obtained for ballistic deposits as initial configuration (see Fig. 4). However, the electron microscope image of carbonyl-iron-powder, Fig. 1, looks differently. It has pores of vastly different sizes. This motivated us to investigate the compaction of a fractal initial configuration. Surprisingly this configuration remains stable to much higher stresses than a ballistic deposit of approximately equal solid fraction. The reason might be the higher coordination number (4 for the (infinite) fractal, but only slightly larger than 2 for the ballistic deposit). However, if the stress is raised above a certain value, the fractal collapses and assumes a similar final configuration as in the case of ballistic deposits (see Fig. 12 and Fig. 14). Then the relation between the volume excess and the stress at the piston is the same for initial configurations that are fractal or ballistic deposits. In the case of the fractal initial condition there is no smooth crossover, but an abrupt transition between an apparently stable constant porosity to the power law decrease, as shown in Fig. 13.

The fractal has a very inhomogeneous mass distribution so that the simple theory for the compaction dynamics developed in Secs. 5 – 8 needs to be modified. Furthermore, even if the stress is large enough to let the fractal collapse, the initial configuration remains nearly unchanged for some time. These simulation results for fractal initial configurations point out an intriguing direction which deserves to be investigated in more detail.

10 CONCLUSIONS AND OUTLOOK

The main results reviewed in this paper are:

• The constitutive law relating the uniaxial consolidation stress σ_y to the compactible volume $V - V_{\rm min}$ is

$$\sigma_y\,(V - V_{\rm min})^{1/\alpha} \sim \frac{F_c}{r^2}\,V_{\rm min}^{1/\alpha} \qquad (26)$$

with a dimensionless proportionality factor. The factor F_c/r^2 implies that nano-powders are much harder

to compactify than micro-powders.
• Experiments with rigid, round particles (carbonyl-iron powders) give an exponent $1/\alpha \approx 2$.
• A sample of compactible volume $V_0 - V_{\min}$ sustains a uniaxial stress, as long as it is far below the corresponding consolidation stress. If one increases the stress slowly, one gets a smooth crossover to a power law decrease of the volume which for quasi-static compaction is given by Eq. (26).
• This constitutive law determines also what constant stress σ_{piston} must be applied to compactify a sample of solid fraction ν_0 to a higher value ν_2 (shock compaction). Due to inertia effects the stress depends on the initial *and* the final volume, V_0 and V_2. According to Eqs. (25) and (26) it is given by

$$\sigma_{\text{piston}} \, (V_2 - V_{\min})^{1/\beta} \sim \sigma_{y,0} \, (V_0 - V_{\min})^{1/\beta} \qquad (27)$$

where $\beta = \alpha(1+\alpha)$, and $\sigma_{y,0}$ is the consolidation stress for the initial solid fraction ν_0.
• In two-dimensional simulations of shock compaction we found the exponent $\beta \approx 3/4$. This corresponds to $1/\alpha \approx 2$ for two-dimensional quasi-static compaction, which happens to be the same as in the three-dimensional experiments.

The theory developed here can be extended in several directions, for example:
• The effect of a finite piston mass could be calculated. When the deceleration front reaches the piston, the powder is at rest, but to stop the piston at the same moment as well, would require an infinite force. Such a force cannot be sustained by the powder, so that another compaction front starts propagating into the powder until the momentum of the piston is used up. This time, however, the piston and hence the compaction front propagate more and more slowly, so that we expect a localized density inhomogeneity near the piston. In our simulations this effect was too weak to be seen right away, so that a more careful study is called for to check this prediction.
• It seems that one can describe the smooth crossover from a constant volume at stresses below the consolidation stress to a power law above by a scaling function. This should be investigated in more detail.

ACKNOWLEDGMENT
We would like to thank our experimental colleagues at the TU Braunschweig, J. Schwedes, M. Morgeneyer and M. Röck, for the enjoyable and inspiring collaboration on this subject. We also thank K. Johnson and G. Bartels for many discussions. Partial support by the German Sience Foundation (SFB 445 and WO577/3), by the German-Israeli-Foundation (795/2003), by the BMBF (HUN 02/011) and by Federal Mogul GmbH is acknowledged.

REFERENCES

Alonso-Marroquín, F. & Herrmann, H. J. 2004. Ratcheting of granular materials. *Phys. Rev. Lett.* 92: 054301.

Bartels, G., Unger, T., Kadau, D., Wolf, D. E., & Kertész, J. 2005. The effect of contact torques on porosity of cohesive powders. *Granular Matter*. cond-mat/0403110.

Brendel, L., Morgeneyer, M., Kadau, D., Schwedes, J., & Wolf, D. E. 2003. Compaction of cohesive powders - a novel description. In *AIDIC Conference Series*: 55. AIDIC & Reed Business Information S.p.A. ISBN 0390-2358.

Brendel, L., Unger, T., & Wolf, D. E. 2004. Contact dynamics for beginners. In *The Physics of Granular Media*: Weinheim: 325. Wiley-VCH.

Hänel, D. & Lantermann, U. 2005. Simulation of particle transport and deposition. In *Traffic and Granular Flow '03*: Heidelberg. Springer.

Heim, L.-O. 2005. private communication (max-planck institute for polymer research, mainz).

Johnson, K. & Wolf, D. E. 2005. Simulation of three dimensional cohesive powder compaction.

Johnson, K. L., Kendall, K., & Roberts, A. D. 1971. Surface energy and the contact of elastic solids. *Proc. Roy. Soc.* A324: 301.

Jullien, R. & Meakin, P. 1989. Concentration effects in the off-lattice random ballistic deposition model. *J. Phys. A: Math. Gen.* 22: L1115.

Kadau, D. 2003. *Porosität in kohäsiven granularen Pulvern und Nano-Pulvern*. Ph. D. thesis: University Duisburg-Essen.

Kadau, D., Bartels, G., Brendel, L., & Wolf, D. E. 2003. Pore stabilization in cohesive granular systems. *Phase Trans.* 76: 315.

Kawakita, K. & Lüdde, K.-H. 1970. Some considerations on powder compression equations. *Powder Technology* 4: 61.

Masteau, J. C., Thomas, G., Chulia, D., & Deleuil, M. 1997. Evolution and modelling of porosity and specific surface area of pharmaceutical tablets during compaction. In *Powders & Grains 97*: Rotterdam. A. A.Balkema.

Morgeneyer, M. 2004. *Mechanische Eigenschaften kohäsiver Schüttgüter*. Ph. D. thesis: Technical Universiy Braunschweig.

Nowak, M. 1994. *Spannungs-/Dehnungsverhalten von Kalkstein in der Zweiaxialbox*. Ph. D. thesis: Technical Universiy Braunschweig.

Radjai, F. & Roux, S. 2004. Contact dynamics study of 2d granular media: Critical states and relevant internal variables. In *The Physics of Granular Media*: Weinheim: 165. Wiley-VCH.

Roscoe, K. H. 1970. Influence of strains in soil mechanics. *Géotechnique* 20: 129.

Schwedes, J. 1975. Shearing behavior of slightly compressed cohesive granular materials. *Powder Technology* 11: 59.

Schwedes, J. 2003. Review on testers for measuring flow properties of bulk solids. *Gran. Mat.* 5: 1.

Srdić, V. V., Winterer, M., & Hahn, H. 2000. Sintering behavior of nanocrystalline zirconia doped with alumina prepared by chemical vapor synthesis. *J. Am. Ceram. Soc.* 83: 1853.

Vold, M. J. 1959. A numerical approach to the problem of sediment volume. *J. Colloid Sci.* 14: 168.